Measurement and modelling of scattering from building walls

Vittorio Degli Esposti*, Franco Fuschini*, Enrico Vitucci*, Daniele Graziani**

*Università di Bologna - Dipartimento di Elettronica, Informatica e Sistemistica
Villa Griffone - 40044 Pontecchio Marconi - Bologna - Italy
e-mail: vdegliesposti@deis.unibo.it, ffuschini@deis.unibo.it, evitucci@deis.unibo.it

**E.S.SAT, Bagnara di Romagna - (RA), Italy
e-mail: info.essat@tiscali.it

[1]ABSTRACT

A measurement campaign aimed at determining the diffuse scattering pattern of typical building walls has been carried out and results are shown in the paper. Such results are then used to determine and tune simple diffuse scattering models based on the Effective Roughness approach, to be embedded into ray tracing simulators. It is shown that by adopting an appropriate single-lobe scattering pattern the agreement between simulation and measurement is very good.

I - INTRODUCTION

Recently, the adoption of Ray Tracing (RT) tools has greatly improved field prediction capabilities in urban environment and good results have been obtained in a variety of cases [1-4]. However, since conventional RT only accounts for rays that undergo specular reflections or diffractions, it fails to properly describe diffuse scattering phenomena which can have a significant impact on propagation. As intended here, diffuse scattering refers to the signals scattered in other than the specular direction as a result of deviations in a building wall from a uniform flat layer (surface or volume irregularities). Recent experimental studies have shown that diffuse scattering plays a fundamental role in determining time and angle dispersion of radio signals in urban environment [5, 6]. The modeling of diffuse scattering from building walls is quite a difficult problem, since building wall irregularities cannot be modeled as Gaussian surface roughness, as assumed in most theoretical studies. Few publications explicitly deal with modeling of diffuse scattering for urban field prediction [7-11]. In particular, in [10] a simple "Effective Roughness" (ER) model for diffuse scattering from building walls has been proposed, and in [11] the same model has been inserted in a 3D ray tracing program, showing a sensible improvement in the accuracy of wideband predictions vs. measurements with respect to conventional RT. The ER model described in [10], however, assumes that the wave impinging on a wall is scattered according to a Lambertian scattering pattern regardless of the direction of incidence.

In the present work the ER model has been modified into a number of versions by orienting in different ways the scattering pattern lobe toward the specular direction, which is more realistic, while preserving physical consistency of the model (section II). Then, the scattering pattern of real building walls has been measured using directive antennas and an appropriate measurement set-up (section III).

Eventually, the experimental scattering patterns have been compared with simulation obtained through the modified ER model embedded into a 3D RT tool (section IV), thus determining the best scattering pattern shape and the best values of the scattering coefficient S in typical cases. Results and conclusions are drawn in sections V and VI, respectively.

II – THE DIFFUSE SCATTERING MODELS

The contribution of diffuse scattering to propagation is evaluated adopting the "Effective Roughness" (ER) approach presented in [10]. A sort of effective roughness is associated with each wall, which not only takes into account real surface roughness but also the wall irregularity effect in a mean, statistical way.

The power scattered by the wall element dS (figure 1) is evaluated as a fraction of the incidence power according to a proper scattering coefficient (S) and the scattered power is spread in all directions as a non uniform spherical wave with amplitude $E_s(\theta_s, \phi_s, r_s)$. According to these assumptions, the following relation must be satisfied

$$S^2 \cdot E_i^2 \cdot d\Omega \cdot r_i^2 = \int_{2\pi} E_s^2 d\Omega = \int_0^{\pi/2} \int_0^{2\pi} E_s^2 \cdot r_s^2 \cdot \sin\theta_s \, d\phi_s d\theta_s \qquad (1)$$

where $d\Omega$ is the solid angle of the ray tube impinging on the surface element dS, E_i is the amplitude of the incident wave and r_i , r_s are the distances between dS and source and reception points, respectively (fig. 1). Introducing the actual assumed shape of the scattered wave E_s (i.e. the scattering pattern) in (1), the absolute value of $E_s(\theta_s, \phi_s, r_s)$ can be derived.

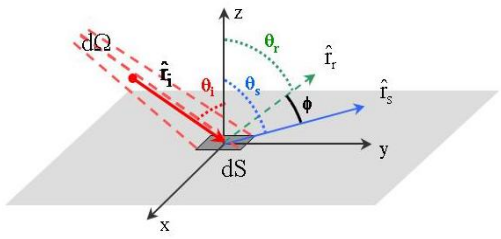

Figure 1 – A generic surface element producing reflection and diffuse scattering

[1]*This work has been carried out within, and partially funded by, the European Network of Excellence* NEWCOM

The shape of the scattering pattern of the wall strongly depends on the characteristics of wall irregularities (windows, balconies, irregular brick, surface roughness, etc.). In order to account for a wide range of possible situations, four different scattering models are hypothesized:

Model 1 (Lambertian model): $E_s = E_{s_0} \cdot \sqrt{\cos\theta_s}$

The "scattering radiation lobe" has its maximum in the direction perpendicular to the wall; the exact expression of E_{s0} can be computed from (1), therefore getting

$$E_s = \frac{K \cdot S}{r_i \cdot r_s} \cdot \sqrt{\frac{\cos\theta_i \cdot \cos\theta_s}{\pi}} dS$$

where K is a constant depending on the amplitude of the impinging wave [10].

In order to steer the scattering lobe in the direction of the specular reflection, the following expression for the amplitude E_s has been considered:

Models 2,3,4: $E_S = E_{S_0} \cdot \left(\frac{1+\cos\phi}{2}\right)^{\alpha/2} \quad \alpha = 1,2,3 \quad (2)$

where ϕ is the angle between the direction of the reflected wave and the scattering direction (θ_s , ϕ_s). Scattering models 2, 3 and 4 have been obtained from (2) for α = 1, 2 and 3, respectively.

According to (2), it is evident that the maximum E_s is achieved for ϕ = 0 (i.e. in the direction of specular reflection); moreover, the greater α, the narrower the scattering lobe. In figure 2, the normalized scattering patterns of models 2,3,4 are shown, for an incidence angle of 30º, with respect to the lambertian model.

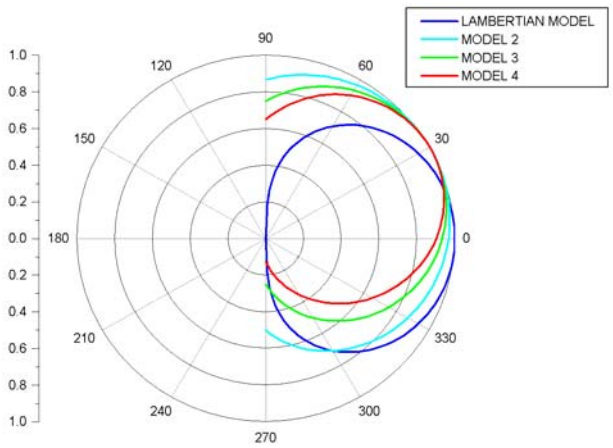

Figure 2 – Comparison of scattering patterns

For each model, the expression E_{s0} can be computed by expressing the ϕ angle in function of the incidence and scattering directions, and then solving equation (1). By means of simple considerations, it is easy to show that:

$$\cos\phi = -(\sin\theta_s \cdot \sin\theta_i) \cdot \cos(\phi_s - \phi_i) + \cos\theta_i \cdot \cos\theta_s$$

In short, the following expressions have been obtained:

- *model 2 (α = 1)*:

$$E_s = \frac{K \cdot S}{r_i \cdot r_s} \sqrt{\frac{dS \cdot \cos\theta_i \cdot (1 - (\sin\theta_s \cdot \sin\theta_i) \cdot \cos(\phi_s - \phi_i) + \cos\theta_i \cdot \cos\theta_s)}{\pi \cdot (2 + \cos\theta_i)}}$$

- *model 3 (α = 2)*:

$$E_s = \frac{K \cdot S}{r_i \cdot r_s} \sqrt{\frac{6 \cdot dS \cdot \cos\theta_i}{\pi \cdot (4 + 3 \cdot \cos\theta_i)}} \cdot \frac{1 - (\sin\theta_s \cdot \sin\theta_i) \cdot \cos(\phi_s - \phi_i) + \cos\theta_i \cdot \cos\theta}{2}$$

- *model 4 (α = 3)*:

$$E_s = \frac{K \cdot S}{r_i \cdot r_s} \sqrt{\frac{8 \cdot dS \cdot \cos\theta_i}{4\pi + 3\pi \cdot \cos\theta_i + \frac{3\pi}{4} \cdot \cos\theta_i \cdot \sin^2\theta_i + \frac{\pi}{2} \cdot \cos^3\theta_i}} \cdot \left(\frac{1 - (\sin\theta_s \cdot \sin\theta_i) \cdot \cos(\phi_s - \phi_i) + \cos\theta_i \cdot \cos\theta}{2}\right)^{3/2}$$

III - THE MEASUREMENT CAMPAIGN

The measurement campaign consists in a set of CW measurements of the power backscattered by 3 different building walls, with the Tx and the Rx equipped with directive antennas oriented toward the center of the wall. Frequency was 1296 MHz, Tx power about 9 dBm, and the total cable losses were of about 5 dB. Three different types of wall have been chosen, each one representative of a different class: a metal, relatively smooth wall of an airport hangar, an uniform brick wall of a warehouse, and a typical brick wall with windows, doors and other elements of a rural building. All walls were nearly the same size of about 10 by 6(height) meters. A parabolic antenna with 1.5 m diameter was used in the Rx, while two different types of antenna were used to illuminate the wall: a circular horn antenna and a parabolic antenna with 1 m diameter. The wall was illuminated in 2 different modes: *normal* incidence (Tx2 in fig. 3) and *slant* incidence (Tx1 and Tx3). It is important to notice that Tx1 and Tx3 are not equivalent, because the radiation pattern of the antennas is not perfectly symmetric.

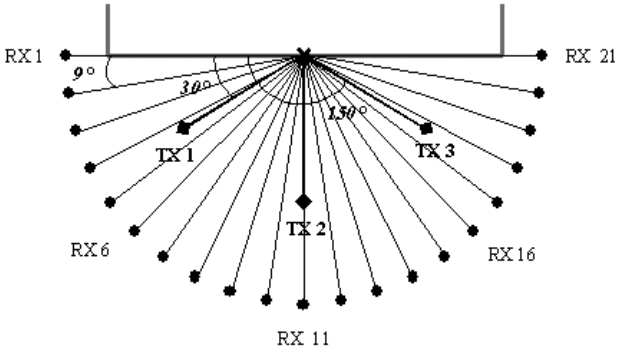

Figure 3 – Tx and Rx positions (top view)

The Rx antenna was positioned on equispaced points (angular separation of 9°) on a semicircle centered in the centre of the wall. Rx antenna and annexed equipment (cables, receiver and a spectrum analyzer) were placed on a mobile carriage, equipped

with an electromechanical pointing system with a video camera.

Finally, in each case, the distance from the wall centre was determined so that the –6 dB main lobe footprint on the wall would be all contained into the wall frame for normal incidence, so as to minimize the effect of the horizontal top edge and of surrounding objects (which were in all cases quite far). The chosen distance was 3.8 m for the horn antenna, 9 m for the 1 m parabolic antenna, and 13 for the 1.5 m parabolic antenna. Tx and Rx antennas were always at a height of 3 m from the ground. Given the relatively small distances, the Rx antenna wasn't in far field w.r.t. the Tx antenna for every Tx/Rx position. However, comparing measurements with RT simulations in reference, free space cases, we observed that deviations due to near field effect were of the order of a few dB's.

IV – THE VALIDATION METHOD

The models proposed in section II are checked with measurements in the following way. Since it is impossible to single out only the diffuse scattering contribution from measurements, due to the limited directivity of the available antennas, we decided to compare measurements with accurate 3D RT simulations of the complete topologies above described, considering the detailed radiation patterns of the antennas (see figure 4). Standard electromagnetic characteristics were used for brick walls (ε_r=5 and conductivity, σ=1.e-2) and of course perfect conductor characteristics for the metal hangar wall. The adopted 3D RT program[11] includes all of the scattering models described in section II and was used here in non-coherent mode, i.e. the contributions coming from direct ray, reflected ray, edge diffracted rays and scattered ray were summed in power. For simplicity, a single scattered ray is computed for each Rx which is assumed to spring from the center of the wall, as in [11] for "far walls". The tuning of the scattering model is quite accurate because the scattering contribution is almost always dominant, except in the specular reflection and in back-to front peaks (see Figures 5 to 10 in section V).

V – RESULTS

Comparisons between measurements and RT predictions, including the ER models proposed above, are shown in this section. All figures show the received power (measured and simulated) vs. Rx angular position. All the antennas used in the measurement campaign have been preliminarily characterized on both the horizontal and the vertical plane. In fig. 4 the horizontal radiation patterns of the Tx antennas (1 m parabolic and horn) are reported, while in fig. 5 the horizontal pattern of the Rx antenna (1,5 m parabolic) is reported. All vertical patterns are omitted, because in all considered cases Tx and Rx antennas are at the same height, and therefore their effect is irrelevant.

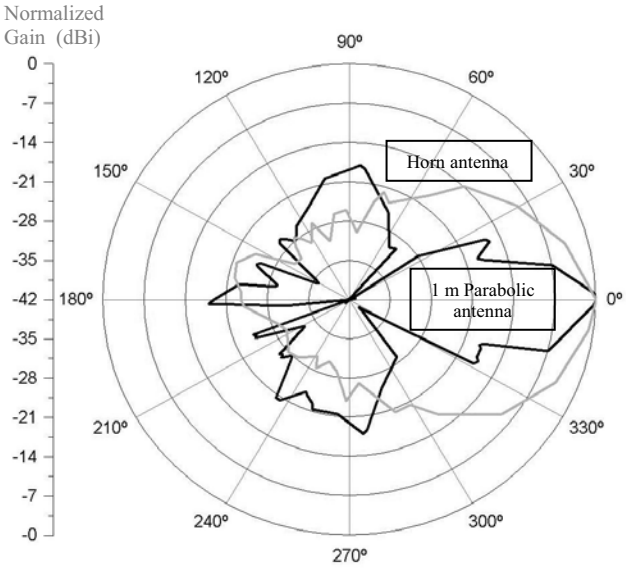

Fig 4 – Tx antennas – Horizontal patterns

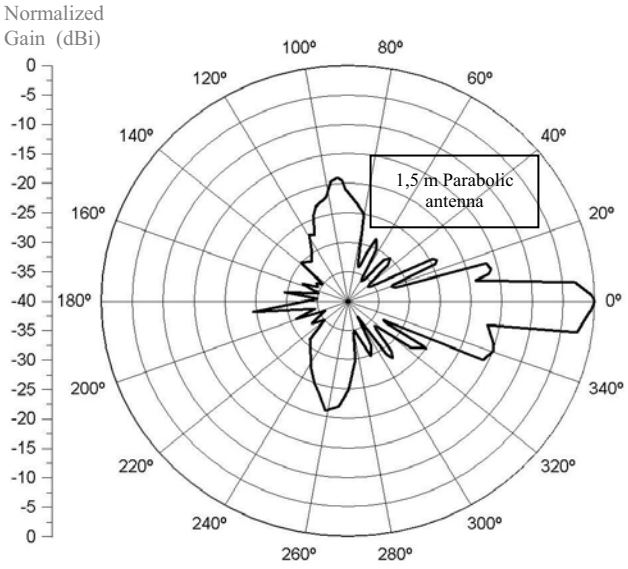

Fig 5 – Rx antenna – Horizontal pattern

In fig. 6 and fig. 7 a comparison between the measurements and the predictions obtained with the different ER versions is shown in the case of the rural building illuminated by a Tx antenna pointed at 150° with respect to the wall plane (position 3 in fig. 3). The former shows the results obtained using the 1 m parabolic antenna as Tx, the latter shows the same result with the horn antenna. For all models, S was set to 3.5. In both cases the best model at minimum squares is model 4. Using model 4 the agreement is very good for Rx's in central positions and Rx's behind the Tx antenna, whereas using the Lambertian model in the same positions the scattered power appears overestimated.

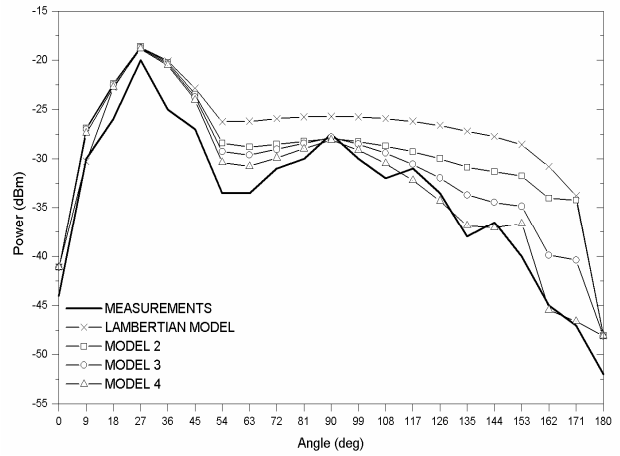

Fig 6 - Comparison of models – Rural building wall illuminated with 1 m parabolic antenna at 150°

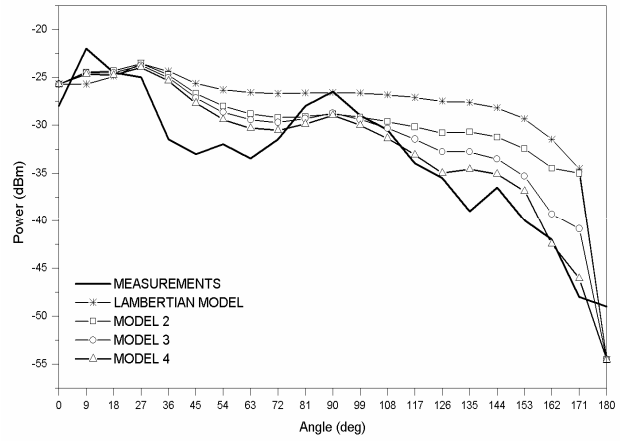

Fig 7 - Comparison of models – Rural building wall illuminated with horn antenna at 150°

In the following figures (8 to 11) comparisons between measurements and predictions for different values of the S parameter are shown: in all cases model 4 is adopted, which demonstrated to be the best in all topologies.

In figures 8 to 10 the results for the hangar wall, the brick wall and the rural building wall are shown, respectively: all measured and simulated values are relative to slant illumination, with 1 m parabolic antenna as Tx. For the hangar wall the Tx antenna was pointed at 30° (Tx position 1 in fig.3), for the brick walls at 150° (Tx position 3). Analogous results have been obtained for normal illumination: in figure 11 the results for the rural building wall, illuminated by the 1 m parabolic antenna perpendicular to the wall, are shown. In all the graphs, the dashed line represents prediction without scattering (S=0).

Fig. 8 shows that for the hangar wall, the predicted power without scattering is slightly underestimated at some points, whereas using S=0.05 a good agreement with measurements is achieved everywhere.

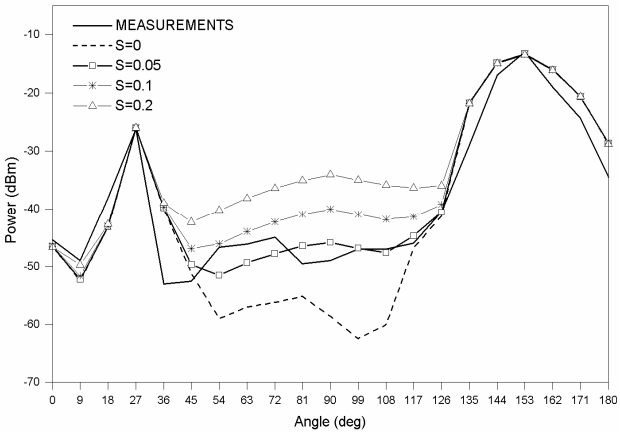

Fig 8 – Hangar wall illuminated with 1 m parabolic antenna at 30°

In fig. 9 it is shown that the best value of S, for the brick wall, is of about 0.2.

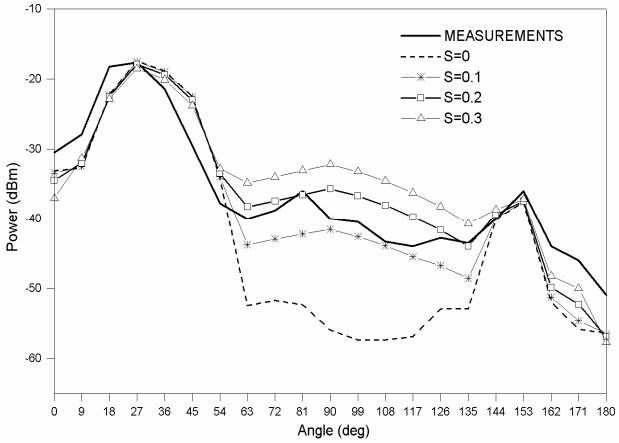

Fig 9 – Brick wall illuminated with 1 m parabolic antenna at 150°

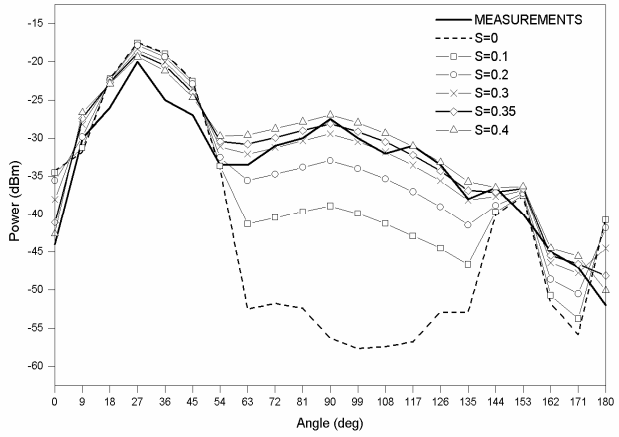

Fig 10 – Rural building wall illuminated with 1 m parabolic antenna at 150°

Finally, figures 10 and 11 show that predictions with S=0 are totally incorrect for a wall belonging to the rural building, which is quite representative of many classes

of real buildings: therefore in such cases the introduction of diffuse scattering is definitely necessary to get a good result. The best value for S is between 0.3 and 0.4 in these cases, in agreement with previous studies [10, 11].

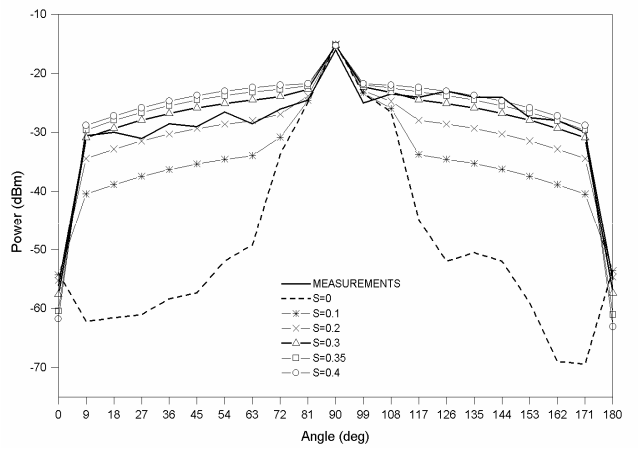

Fig 11 – Rural building wall illuminated with 1 m parabolic antenna at 90°

VI - CONCLUSIONS

A measurement campaign aimed at determining the scattering pattern of typical building walls is reported in the paper. In addition, the diffuse scattering ER model is modified and tuned in order to get the best agreement with measurements. It is shown that "model 4" is the best in all cases, and the optimum scattering coefficient S values are of 0.1, 0.2 and 0.35 in the three considered topologies considered, respectively. Being the latter topology quite representative of simple, brick-wall suburban buildings, we can infer that S=0.35 is the recommended value for field prediction in suburban areas, in agreement with previous work [10, 11]. Simulations in dense urban environment would probably require even greater values of S, i.e. greater diffuse scattering contribution.

VII - ACKNOWLEDGEMENTS

The Authors would like to thank the association "Centro Radioastronomico Bagnara di Romagna" for the useful suggestions and for the support in performing the measurements reported in the paper.

REFERENCES

[1] T. Kürner, D. J. Cichon and W. Wiesbeck, "Concepts and results for 3D digital terrain-based wave propagation models: an overview," IEEE Journal on Selected Areas in Communications, Vol. 11, No. 7, pp.1002-1012, September 1993.

[2] M. C. Lawton and J. P. McGeehan, "The application of a deterministic ray launching algorithm for the prediction of radio channel characteristics in small-cell environments," IEEE Trans. Veh. Technol., vol. 43, pp.955-969, Nov. 1994.

[3] G. Liang and H. L. Bertoni , "A new approach to 3D ray tracing for propagation prediction in cities," IEEE Trans. Ant. Propagat., vol. 46, no. 6, pp.853-863, June 1998.

[4] Hsueh-Jyh Li, Cheng-Chung Chen, Ta-Yung Liu, Han-Chang Lin, "Applicability of ray-tracing technique for the prediction of outdoor channel characteristics," IEEE Transactions on Vehicular Technology, Volume: 49 , Issue: 6 , Pages:2336 – 2349, Nov. 2000.

[5] K. Kalliola, H. Laitinen, P. Vainikainen, M. Toeltsch, J. Laurila, E. Bonek, "3-D double-directional radio channel characterization for urban macrocellular applications," IEEE Transactions on Antennas and Propagation, Vol. 51, No. 11, Pages:3122 - 3133, November 2003.

[6] J. Laurila, K. Kalliola, M. Toeltsch, K. Hugl, P. Vainikainen, E. Bonek, "Wideband 3-D characterization of mobile radio channels in urban environment," IEEE Transactions on Antennas and Propagation, Vol. 50, No. 2, Pages:233 - 243, February 2002

[7] M. O. Al-Nuaimi and M. S. Ding, "Prediction models and measurements of microwave signals scattered from buildings," IEEE Trans. Ant. Propagat., vol. 42, no. 8, pp.1126-1137, August 1994.

[8] C. Kloch, J. Bach Andersen, "Radiosity - an approach to determine the effect of rough surface scattering in mobile scenarios", IEEE AP-S International Symposium, pp 890-893, Montreal, July 1997.

[9] D. Didascalou, M. Dottling, N. Geng, W. Wiesbeck, "An approach to include stochastic rough surface scattering into deterministic ray-optical wave propagation modeling," IEEE Transactions on Antennas and Propagation, Volume: 51 , Issue: 7 , Pages:1508 – 1515, July 2003.

[10] V. Degli-Esposti, "A diffuse scattering model for urban propagation prediction," IEEE Transactions on Antennas and Propagation, Vol. 49, No. 7, pp. 1111-1113, July 2001.

[11] V. Degli Esposti, D. Guiducci, A. de'Marsi, P. Azzi, F. Fuschini, "An advanced field prediction model including diffuse scattering," IEEE Transactions on Antennas and Propagation, Vol. 52, No. 7, Pages:1717 - 1728, July 2004.